

Effects of anharmonic strain on phase stability of epitaxial films and superlattices: applications to noble metals

V. Ozolins, C. Wolverton, and Alex Zunger
National Renewable Energy Laboratory, Golden, CO 80401
(September 12, 1997)

Epitaxial strain energies of epitaxial films and bulk superlattices are studied via first-principles total energy calculations using the local-density approximation. Anharmonic effects due to large lattice mismatch, beyond the reach of the harmonic elasticity theory, are found to be very important in Cu/Au (lattice mismatch 12%), Cu/Ag (12%) and Ni/Au (15%). We find that h001i is the elastically soft direction for biaxial expansion of Cu and Ni, but it is h201i for large biaxial compression of Cu, Ag, and Au. The stability of superlattices is discussed in terms of the coherency strain and interfacial energies. We find that in phase-separating systems such as Cu-Ag the superlattice formation energies decrease with superlattice period, and the interfacial energy is positive. Superlattices are formed easiest on (001) and hardest on (111) substrates. For ordering systems, such as Cu-Au and Ag-Au, the formation energy of superlattices increases with period, and interfacial energies are negative. These superlattices are formed easiest on (001) or (110) and hardest on (111) substrates. For Ni-Au we find a hybrid behavior: superlattices along h111i and h001i behave like in phase-separating systems, while for h110i they behave like in ordering systems. Finally, recent experimental results on epitaxial stabilization of disordered Ni-Au and Cu-Ag alloys, immiscible in the bulk form, are explained in terms of destabilization of the phase separated state due to lattice mismatch between the substrate and constituents.

PACS numbers: 62.20.Dc, 68.60.-p, 81.10.Aj

I. INTRODUCTION

Recently, there has been much interest¹⁻¹⁴ in growth of epitaxial metal films and superlattices due to their unusual physical properties. The quality and structure of these systems is of paramount importance for applications. Epitaxial monolayer and multilayer (up to 10 layers) formation has been observed for many metal/semiconductor and metal/metal combinations. Most metal/metal superlattices have been grown for elements in different crystal structures (e.g., fcc/bcc) and with considerable size mismatch (e.g., 10% for Cu/Nb¹⁵⁻¹⁷). Furthermore, elemental metals and alloys have been found to form epitaxially in structures which are unstable in bulk form.¹⁸⁻²² Recently, the topic of surface alloy formation in bulk immiscible systems has attracted considerable attention.²³⁻⁴² These systems are usually strained due to film/substrate lattice mismatch. One would like to understand and predict the stability of these types of strained materials. In order to do so, one requires knowledge of two types of energies. The stability of epitaxial $A_{1-x}B_x$ alloy films and strained A_pB_q superlattices depends on (i) the energies of coherently strained constituents A and B, and (ii) the formation energy of $A_{1-x}B_x$ or A_pB_q itself. Regarding (i), previous theoretical studies^{18,43-56} have described these energies using harmonic models, but we are interested here in large strains for which the harmonic theory could break down. Thus, we develop a generalization of previous methods to treat the anharmonic epitaxial strain energies of the con-

stituents. Regarding (ii), these energies depend on the conformation degrees of freedom of the epitaxial film, so their calculation requires statistical methods.^{56,57} In the present paper we investigate items (i) and (ii) above using accurate first-principles LDA calculations.

As for (i), the constituent strain energy, we find that the harmonic strain theory,^{18,46} predicting a single, universal relation for elastically soft directions, breaks down for sufficiently large substrate/film lattice mismatch. We find that under biaxial expansion, noble metals are soft along h001i, but that under compression the soft direction changes to h201i. It is shown that the softness of h001i is a consequence of low bcc/fcc energy differences in noble metals, while the softness of h201i under compressive strain can be explained by loose packing of atoms in the f201g planes. Furthermore, the elastic strain energy as a function of direction exhibits qualitative shifts in the hard and soft strain directions, which cannot be guessed from the harmonic elasticity theory. For instance, we find that h110i becomes the hardest direction under biaxial expansion, and h201i becomes the softest direction under biaxial compression, while the harmonic theory always predicts either h111i as the hardest and h001i as the softest direction, or vice versa.

Regarding (ii), the formation energy, we find that the anomalous elastic softness of the constituents along h001i and h201i leads to low constituent strain energy in superlattices along these directions, which makes them more stable than superlattices along other Φ . For instance, in the size-mismatched systems Cu-Au, Cu-Ag, and Ni-Au,

A_nB_n superlattices along $h001i$ are the most stable for all periods n . Interfacial energies are found to be negative in Ag-Au and Cu-Au (reflecting their bulk miscibility), and positive in the phase separating systems Cu-Ag and Ni-Au. However, attraction between (110) interfaces in Ni-Au is very strong and favors short-period ($n/2$) superlattices over long-period superlattices with few interfaces.

In the case of epitaxially grown disordered alloys, we find that the biaxial constraint on the phase separated constituents may stabilize the alloy with respect to phase separation. The stabilization effect is always greater on substrates oriented along elastically hard directions (i.e., with high constituent strain energy) like $h111i$ than along soft directions like $h001i$. For instance, on lattice-matched substrates, epitaxial $Ni_{0.5}Au_{0.5}$ alloys are stable at all temperatures, and $Cu_{0.5}Ag_{0.5}$ alloys are stable for $T > 150$ K if grown on a (111) substrate, although both these systems phase separate in bulk form or if grown on a (001) substrate. These predictions agree very well with recent experimental observations.^{31;36}

II. BULK AND EPITAXIAL STABILITY CRITERIA

The stability of either free-standing or coherently strained alloys and superlattices requires specification of (i) epitaxial strain energies of pure constituents due to

\ln /substrate lattice mismatch, (ii) formation enthalpies of disordered alloys (with respect to either strained or unstrained bulk constituents) and superlattices. In this section, we define these quantities and discuss the physical situations where they should be used.

A. Epitaxial strain energies of elemental constituents

We start by considering (i) above, which is a common element to alloys and superlattices. Consider a \ln of pure element A coherently strained on a substrate oriented along direction Φ with surface unit cell vectors a_1 and a_2 , orthogonal to Φ . We assume that the \ln , being much thinner than the substrate, maintains coherency with the substrate and plastically deforms to accommodate the lattice mismatch at the interface. This assumption is valid for \ln s thinner than the critical thickness for the nucleation of misfit dislocations. Furthermore, we consider \ln s which are thick enough so that the chemical interaction energy at the \ln /substrate interface and \ln /vacuum surface is negligibly small in comparison with the elastic deformation energy of the \ln .

Under these assumptions, the epitaxial strain energy $E_A^{\text{epi}}(a_1; a_2; \Phi)$ of \ln A is the strain energy of element A deformed in the growth plane to the unit cell vectors $fa_1; a_2g$ of the substrate, and relaxed with respect to the out-of-plane vector c :

$$E_A^{\text{epi}}(a_1; a_2; \Phi) = \min_c E_A^{\text{tot}}(a_1; a_2; c) - E_A^{\text{tot}}(a_A) : (1)$$

In what follows, we are interested in the case where both the substrate and the unstrained bulk element A have the fcc crystal lattice. Then a_1 and a_2 are proportional to the equilibrium unstrained lattice vectors of fcc A, $a^0_1(A)$:

$$a_i = \frac{a_s}{a_A} a^0_i(A); \quad i = 1, 2; \quad (2)$$

where a_s and a_A are fcc lattice parameters of the substrate and A, correspondingly. The epitaxial strain energy becomes a function of the substrate lattice constant and direction Φ only:

$$E_A^{\text{epi}}[(a_s=a_A)a_1; (a_s=a_A)a_2; \Phi] = E_A^{\text{epi}}(a_s; \Phi) : (3)$$

LDA calculations of $E_A^{\text{epi}}(a_s; \Phi)$ are described in Sec. III.

B. Formation enthalpies of alloys and superlattices

Like the formation enthalpy of any ordered bulk compound, the formation enthalpy $H_{\text{SL}}^{\text{bulk}}(pq; \Phi)$ of an A_pB_q unstrained (bulk) superlattice is defined as the energy gain or loss with respect to unstrained bulk constituents:

$$H_{\text{SL}}^{\text{bulk}}(pq; \Phi) = E^{\text{tot}}(A_pB_q; \Phi) - \frac{p}{p+q} E_A^{\text{tot}}(a_A) - \frac{q}{p+q} E_B^{\text{tot}}(a_B) ; \quad (4)$$

where a_A is the equilibrium lattice constant of the unstrained bulk element A and $E_A^{\text{tot}}(a_A)$ is the total energy of A. This enthalpy characterizes the propensity to form superlattices with respect to the phase separated bulk constituents. If $H_{\text{SL}}^{\text{bulk}}(pq; \Phi) < 0$, the unstrained superlattices are energetically favored over the phase separation, while the phase separated state is favored if $H_{\text{SL}}^{\text{bulk}}(pq; \Phi) > 0$. To be stable, free-standing bulk superlattices must satisfy stability criteria with respect to at least: (i) phase separation into unstrained bulk constituents and (ii) formation of a configurationally disordered bulk alloy. The bulk mixing enthalpy, $H_{\text{mix}}^{\text{bulk}}(A_1-xB_x)$, of the alloy is given by:

$$H_{\text{mix}}^{\text{bulk}}(A_1-xB_x) = E^{\text{tot}}(A_1-xB_x) - (1-x)E_A^{\text{tot}}(a_A) - xE_B^{\text{tot}}(a_B) ; \quad (5)$$

where $x = q/(p+q)$ is the composition and $E^{\text{tot}}(A_1-xB_x)$ is the total energy per atom of the configurationally random alloy.

If $H_{\text{mix}}^{\text{bulk}}(A_1-xB_x) < H_{\text{SL}}^{\text{bulk}}(A_pB_q) < 0$, then both the superlattice and disordered alloy are stable with respect to phase separation, but the superlattice is unstable with respect to disordering. However, if

$H_{SL}^{bulk}(A_p B_q) < H_{mix}^{bulk}(A_{1-x} B_x) < 0$, then superlattices are stable with respect to both phase separation and disordering, and it may be possible to grow them.

The bulk formation enthalpy of a superlattice, $H_{SL}^{bulk}(pq; \phi)$, can be separated into two components. To identify them, it is useful to first consider the infinite period superlattice limit $p; q \rightarrow \infty$, where $A=B$ interfacial interactions contribute a negligible amount of order $O(1/p)$. In this case, the bulk formation enthalpy of $A_{1-x} B_x$ superlattice is given by

$$H_{SL}^{bulk}(pq; \phi) = H_{CS}^{eq}(x; \phi) + \lim_{n \rightarrow \infty} \frac{1}{n} \sum_{a_1, a_2} (1-x) E_A^{epi}(a_1; a_2; \phi) + x E_B^{epi}(a_1; a_2; \phi); \quad (6)$$

where E_A^{epi} is the epitaxial deformation energy of A, given by Eq. (1). We define this energy as the "constituent strain" (CS) to emphasize that in this limit the superlattice formation enthalpy depends only on its strained constituents. This is also the energy required to keep A and B coherent.

For finite-period superlattices, the formation energy is determined not only by the elastic strain energy, but also by interactions between unlike atoms at $A=B$ interfaces. We define this interfacial energy $I(pq; \phi)$ as:

$$H_{SL}^{bulk}(pq; \phi) = H_{SL}^{bulk}(pq; \infty; \phi) + \frac{4}{p+q} I(pq; \phi); \quad (7)$$

It is the total energy per layer of a single interface between infinite slabs of A and B oriented along ϕ . $I(1) < 0$ signals that the interface is energetically favored, while $I(1) > 0$ indicates that an isolated interface is not preferred, and long-period superlattices with fewer interfaces are usually more stable than the short-period ones (however, this simple argument is not always true, see the following discussion).

For equiatomic $(A)_n = (B)_n$ superlattices Eq. (7) becomes:

$$H_{SL}^{bulk}(n; \phi) = \frac{2I(n; \phi)}{n} + E_{CS}^{eq}(x=0.5; \phi); \quad (8)$$

For small n interfaces will interact with each other. We describe this process by the interface interaction energy $I(n; \phi)$:

$$I(n; \phi) = I(n; \phi) - I(n-1; \phi); \quad (9)$$

Negative $I(n; \phi)$ may favor short-period superlattices over long-period superlattices even if the interfacial energy $I(n-1; \phi)$ is positive. For this to happen it is necessary that

$$I(n; \phi) < -I(n-1; \phi); \quad (10)$$

In Sec. IV C we show that this unusual phenomenon occurs in NiAu.

If a disordered alloy is grown epitaxially on a lattice-matched fcc substrate, its stability with respect to phase separation is given by the epitaxial mixing enthalpy:

$$H_{mix}^{epi}(A_{1-x} B_x) = H_{mix}^{bulk}(A_{1-x} B_x) + (1-x) E_A^{epi}(a_s; \phi) + x E_B^{epi}(a_s; \phi); \quad (11)$$

where $E_A^{epi}(a_s; \phi)$ is the epitaxial strain energy of Eq. (3), accounting for the fact that the phase-separated constituents must also be lattice-matched with the substrate. Due to the presence of these terms, disordered alloys may form epitaxially [$H_{mix}^{epi}(A_{1-x} B_x) < 0$] even if the corresponding bulk alloys phase separate [$H_{mix}^{bulk}(A_{1-x} B_x) > 0$]. This situation is especially likely to occur for elastically hard directions ϕ with large values of $E_{A,B}^{epi}(a_s; \phi)$, for instance $h11\bar{1}$ and $h10\bar{1}$ (see Sec. III B).

The objective of this work is to calculate $H_{SL}^{bulk}(A_p B_q)$ [Eq. (4)], $H_{mix}^{bulk}(A_{1-x} B_x)$ [Eq. (5)] and $H_{mix}^{epi}(A_{1-x} B_x)$ [Eq. (11)] from first principles for AgAu, CuAg, CuAu, and NiAu. This requires:

(a) Epitaxial strain energies of pure constituents, $E_A^{epi}(a_s; \phi)$ [Eq. (3)], for Ag, Au, Cu and Ni. This is described in Sec. III.

(b) Equilibrium constituent strain energy E_{CS}^{eq} [Eq. (6)] for AgAu, CuAg, CuAu, and NiAu. This is described in Sec. IV A.

(c) The interfacial energy $I(pq; \phi)$ of Eq. (8) requires $H_{form}^{bulk}(A_p B_q; \phi)$ for arbitrary pq and ϕ . $H_{mix}^{bulk}(A_{1-x} B_x)$ and $H_{mix}^{epi}(A_{1-x} B_x)$ require the total energy of a compositionally disordered solid solution. All these quantities are obtained from the mixed-space cluster expansion as described in Sec. IV B.

III. ELEMENTAL EPITAXIAL FILMS

A. Anharmonic epitaxial strain in thin films of pure elements: Analytic forms

The epitaxial strain energy [Eq. (3)] of a film of element A (with an equilibrium fcc lattice constant a_A) on a fcc substrate with lattice constant a_s , oriented along direction ϕ , is conveniently obtained in a two-step process considered by Hornstra and Bartels.⁴³ First, the fcc crystal of bulk A is uniformly stretched (or compressed) to the lattice constant of the substrate a_s . The energy change relative to free A is given by the hydrostatic bulk deformation energy $E_A^{bulk}(a_s)$. In the second step, out-of-plane unit cell vector c of the film relaxes to satisfy Eq. (1). The change $c = c_0 (a_s/a_A)^{c^0}$ (where c^0 is the fcc lattice vector of unstrained A), has components parallel [c_k] and perpendicular [c_\perp] to the growth direction ϕ . The parallel component c_k changes the volume of the unit cell and thus has a large effect on the total energy. In contrast, the so-called shear strain c_\perp shifts

planes orthogonal to Φ and does not change the volume of the unit cell. Consequently, it has a much smaller effect on the total energy. Furthermore, this strain vanishes by symmetry for directions $h00i$, $h11i$ and $h10i$, and the shear strain energy must have zero angular derivatives at these points. Therefore, we neglect the shear strain ϵ_{γ} also for low-symmetry directions. Bottomley and Fons⁴⁶ have shown that this approximation introduces rather small errors in the harmonic epitaxial strain energies.

Neglecting the shear strain ϵ_{γ} , the strain energy of element A is then a function of the direction Φ and two scalar variables, a_s and $k = j c_k / a_s - 1$. The epitaxial strain energy $E_A^{\text{epi}}(a_s; \Phi)$ of Eq. (3) is the minimum of the strain energy with respect to k at a fixed substrate lattice constant a_s :

$$E_A^{\text{epi}}(a_s; \Phi) = \min_k E_A^{\text{tot}}(a_s; k; \Phi) - E_A^{\text{tot}}(a_A): \quad (12)$$

The epitaxial strain energy $E_A^{\text{epi}}(a_s; \Phi)$ is related to the epitaxial softening function^{53;18} $q(a_s; \Phi)$ by the relation:

$$q(a_s; \Phi) = \frac{E_A^{\text{epi}}(a_s; \Phi)}{E_A^{\text{bulk}}(a_s)}; \quad (13)$$

where $E_A^{\text{bulk}}(a_s)$ is the hydrostatic deformation energy of fcc A to the substrate lattice constant a_s . The function Eq. (13) quantifies energy lowering due to the relaxation of c (A) in the second step of the deformation process considered above.

The harmonic elasticity theory without the shear strain gives^{18;56;46} $q_{\text{ham}}(\Phi)$ which depends on the growth direction Φ but not on the substrate lattice constant a_s :

$$q_{\text{ham}}(\Phi) = 1 - \frac{B}{C_{11} + q_{\text{ham}}(\Phi)}; \quad (14)$$

where $B = \frac{1}{3}(C_{11} + 2C_{12})$ is the bulk modulus, $\alpha = C_{44} / \frac{1}{2}(C_{11} - C_{12})$ is the elastic anisotropy parameter, and $q_{\text{ham}}(\Phi)$ is a geometric function of the spherical angles formed by Φ :

$$\begin{aligned} q_{\text{ham}}(\Phi) &= \sin^2(2\theta) + \sin^4(\theta) \sin^2(2\phi) \\ &= \frac{4\alpha}{5} \left[\frac{1}{4} K_0(\Phi) - \frac{2}{21} K_4(\Phi) \right]; \end{aligned} \quad (15)$$

K_1 is the Kubic harmonic of angular momentum 1. The equilibrium value of the $\alpha_k = a/a_A$ ratio of the film is given by

$$c_k^{\text{eq}}(a_s; \Phi) = a_s(1 + \alpha_k) = a_A [2 - 3q_{\text{ham}}(\Phi)](a_s/a_A): \quad (16)$$

For the principle high-symmetry directions we have

$$q_{\text{ham}}([001]) = 0; \quad q_{\text{ham}}([110]) = 1; \quad q_{\text{ham}}([111]) = \frac{4}{3}: \quad (17)$$

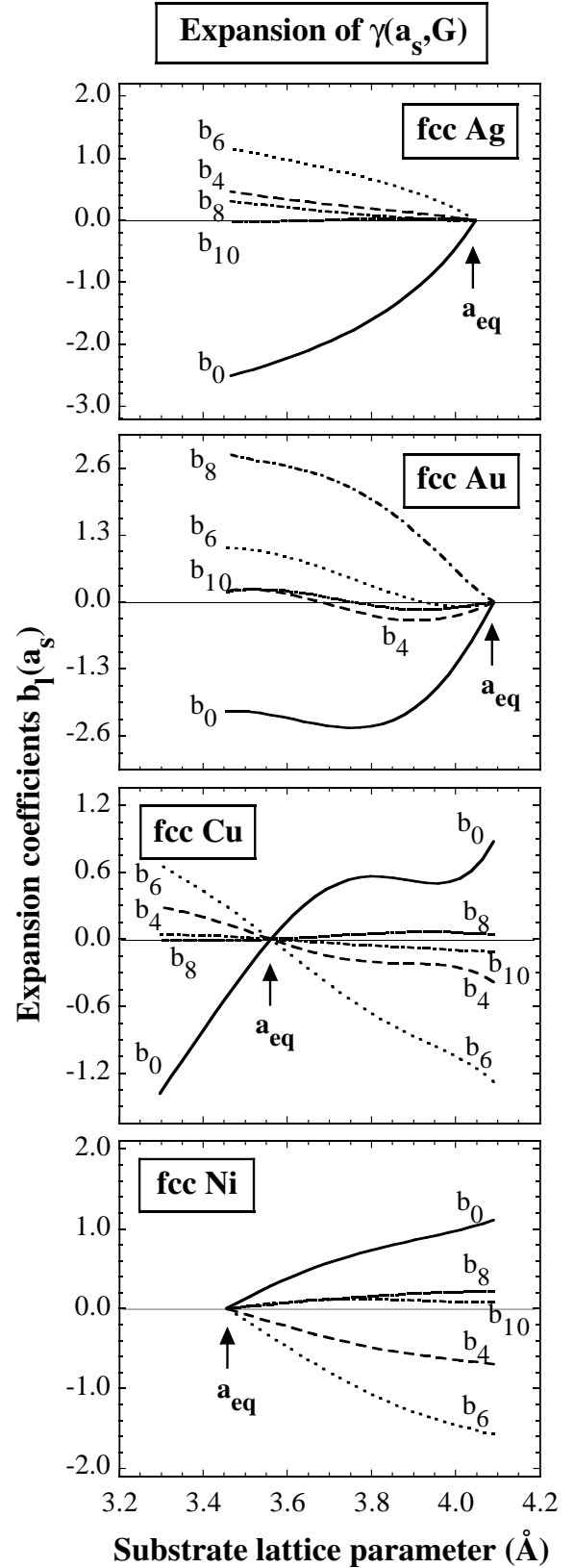


FIG. 1. Expansion coefficients $b_l(a_s)$ of Eq. (18) for Ag, Au, Cu, and Ni.

A parametric plot of q is presented in Ref. 56, which shows that the minimum of $q(\phi)$ is along $h001i$ and the maximum q along $h111i$. Therefore, depending on the sign of the elastic anisotropy, $q_{\text{ham}}(\phi)$ is either lowest for the $h001i$ direction, and then $q_{\text{ham}}([111])$ is the highest, or vice versa. Other directions always have intermediate values of $q_{\text{ham}}(\phi)$.

If anharmonic effects are important, q becomes a function of the substrate lattice parameter a_s . As we will show in Sec. IIIB, for deformations $2(a_s - a_A)/(a_s + a_A)$ of approximately 4%, the "exact" LDA $q(a_s; \phi)$ exhibits appreciable dependence on the substrate lattice parameter a_s and certain qualitative features cannot be reproduced by the harmonic functional form Eqs. (14)-(15). Furthermore, sufficiently large epitaxial strains may take the lattice from the face-centered cubic (fcc) structure into other low-energy structures [e.g., body-centered cubic (bcc) and body-centered tetragonal (bct)], causing anomalous softening of $q(a_s; \phi)$ for these directions. Section IIIB shows that this indeed happens for $h001i$ epitaxial strain when $a_s > a_A$. Therefore, Eqs. (14)-(15) must be generalized to account for nonlinear effects beyond the reach of the harmonic theory. This is achieved by replacing in Eq. (14) $q_{\text{ham}}(\phi)$ by $q(a_s; \phi)$, where

$$q(a_s; \phi) = q_{\text{ham}}(\phi) + \sum_{l=0}^{\infty} b_l(a_s) K_l(\phi) \quad (18)$$

includes higher Kubic harmonics. For cubic systems $l=0; 4; 6; 8; \dots$. The general expression for q is

$$q(a_s; \phi) = 1 - \frac{B}{C_{11} + (a_s; \phi)} : \quad (19)$$

We have chosen this particular form for q since it guarantees that all expansion coefficients tend to zero in the harmonic limit:

$$\lim_{a_s \rightarrow a_A} b_l(a_s) = 0 : \quad (20)$$

In summary, to calculate $E^{\text{epi}}(a_s; \phi)$ of Eq. (3) we will use Eq. (12) to obtain it from LDA for a few substrate lattice parameters a_s and along selected symmetry directions ϕ . We will also need to obtain the harmonic elastic constants C_{11} , C_{12} and C_{44} . The calculated $E^{\text{epi}}(a_s; \phi)$ results are then fitted by the general Eqs. (13), (18) and (19).

B. Anharmonic epitaxial strain of thin films of pure elements: LDA results

We have calculated the epitaxial strain energy $E^{\text{epi}}(a_s; \phi)$ for Cu, Ni, Ag and Au along six principle directions $h001i$, $h111i$, $h110i$, $h113i$, $h201i$ and $h221i$. The local-density approximation⁵⁸ (LDA), as

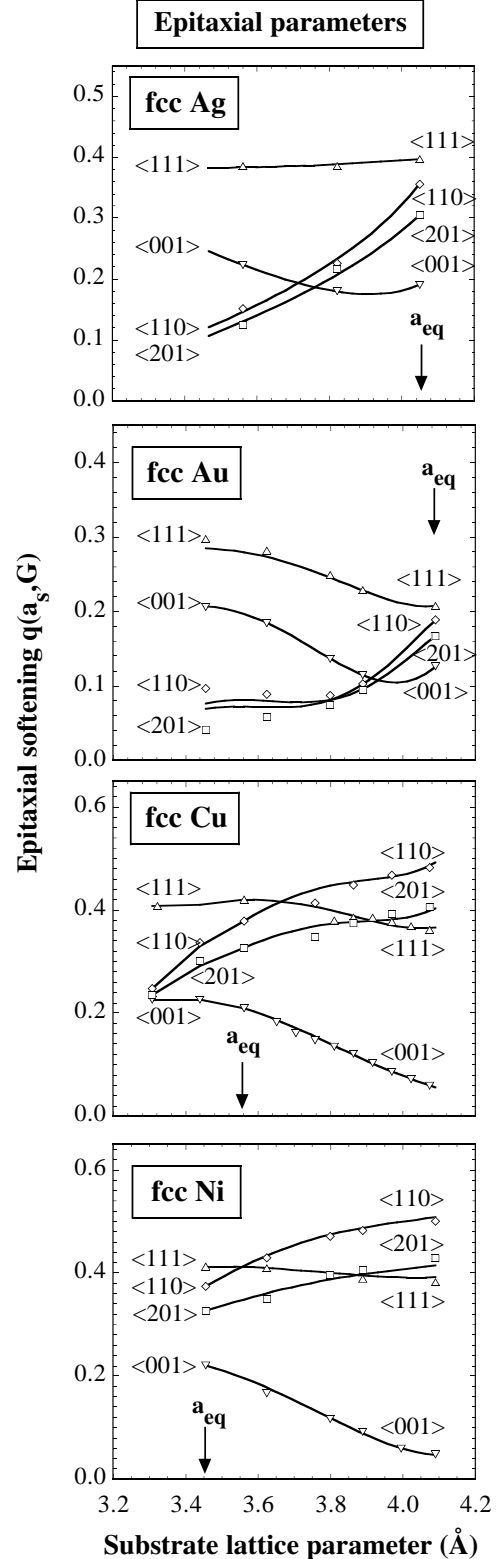


FIG. 2. The calculated epitaxial softening functions $q(a_s; \phi)$ for Cu, Ni, Ag and Au. Points represent the directly calculated LDA values and lines show the fit using Eqs. (19)-(18).

Epitaxial softening $q(a_s, G)$

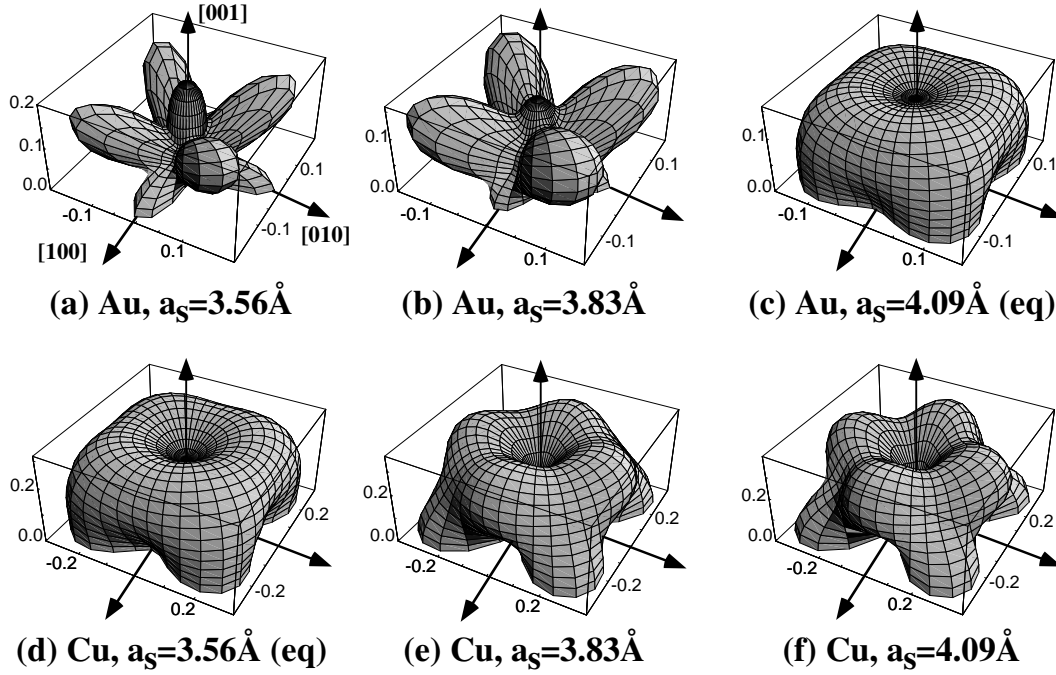


FIG. 3. Epitaxial softening function $q(a_s; \Phi)$ for (a)-(c) Cu and (d)-(f) Au, at different values of the substrate lattice constant a_s .

implemented by the linearized augmented plane wave (LAPW) method⁵⁹, was used to obtain the total energies in Eqs. (12) and (13). $q(a_s; \Phi)$ was calculated from Eq. (13) and fitted with the functional form Eqs. (18)-(19). The angular momentum cutoff in Eq. (18) was set to $l_{\text{max}} = 10$, leaving five independent coefficients for each value of the substrate lattice parameter a_s . This choice allows reproduction of the LDA values with a maximum error of 0.04. The calculations have been done for biaxial compression ($a_s < a_{\text{eq}}$) of Au and Ag, for biaxial expansion and compression of Cu. The expansion coefficients $b_l(a_s)$, entering Eqs. (18), are shown in Fig. 1. At the equilibrium lattice constant a_{eq} (vertical arrows in Fig. 1), where the harmonic formula Eq. (15) is exact, all b_l are exactly zero. As a_s deviates from a_{eq} , they change rapidly indicating the importance of anharmonic effects. In Cu and Ni for $a_s > a_{\text{eq}}$, $l=6$ term is as important as $l=0$ and $l=4$ terms, contributions from $l=8$ being an order of magnitude smaller. In Au for $a_s < a_{\text{eq}}$, $b_0(a_s)$ and $b_8(a_s)$ are the dominating terms, while the behavior of Ag is mainly determined by $b_0(a_s)$ and $b_6(a_s)$. Thus, in spite of broad similarities between the studied elements, they exhibit some interesting differences.

Figure 2 shows the calculated LDA epitaxial softening functions $q(a_s; \Phi)$ of Eq. (13) for Cu, Ni, Ag and Au. There are important qualitative and quantitative differ-

ences between $q_{\text{harm}}(\Phi)$ given by the harmonic elasticity Eq. (14), and the anharmonic $q(a_s; \Phi)$ calculated from the LDA. First, all $q(a_s; \Phi)$ depend on the substrate lattice constant a_s , while the harmonic $q_{\text{harm}}(\Phi)$ are independent of a_s . Figure 3 shows the directional dependence of $q(a_s; \Phi)$ for Cu and Au at a few values of a_s : equilibrium lattice parameter of Cu (3.56 Å), equilibrium lattice parameter of Au (4.04 Å), and halfway between them (3.83 Å). By construction, q at $a_s = a_{\text{eq}}$ is given by the harmonic form Eqs. (14)-(15), shown for fcc Au in Fig. 3(c) and fcc Cu in Fig. 3(d). Epitaxial deformation of Au with $a_s < a_{\text{eq}}$ makes the lobes along $h111i$ much more pronounced than in the harmonic case. Furthermore, q for Au develops additional lobes along $h001i$, which in the harmonic approximation is the softest direction. In contrast, q of Cu under biaxial expansion exhibits pronounced deepening of the $h001i$ minimum, but develops maxima along $h110i$.

Second, in the harmonic elasticity theory of Eq. (14) if $h001i$ is the softest direction (smallest q_{harm}), then $h111i$ must be the hardest direction, and vice versa. Figure 2 shows that this order does not hold for large deformations: the hardest direction in Ni and Cu for $a_s = a_{\text{eq}}$ is $h110i$, while the hardest directions in Ag and Au for $a_s = a_{\text{eq}}$ are $h111i$ and $h001i$, both $h110i$ and $h201i$ being much softer than the former.

Epitaxial (100) strain energy of Cu

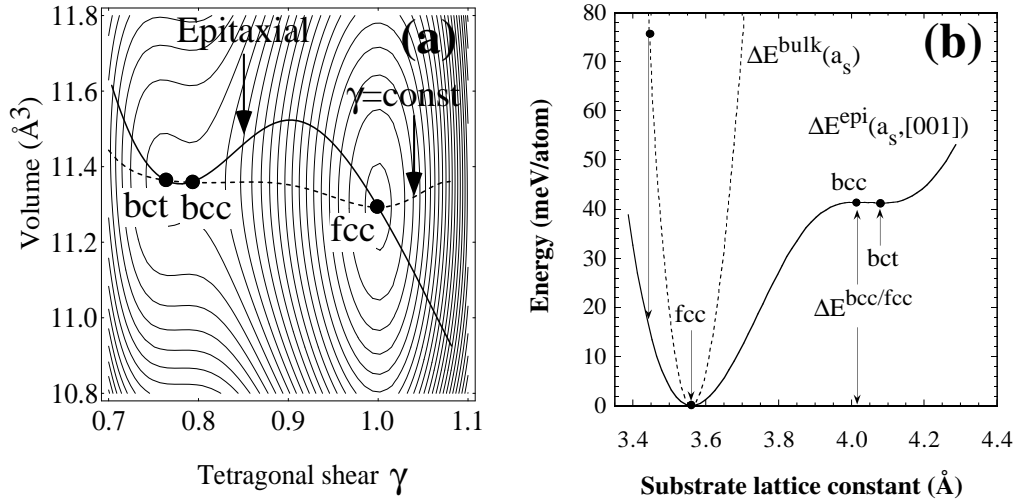


FIG. 4. Contour plot of the two-dimensional energy surface $E(\gamma; V)$ for Cu. The continuous line shows the epitaxial path determined by Eq. (23), while the dashed line is the relation $V = V(\gamma)$ obtained by minimizing $E(\gamma; V)$ with respect to the volume V at a constant γ . The right panel shows the epitaxial strain energy as a function of the substrate lattice constant in comparison with the (much larger) bulk deformation energy $E^{\text{bulk}}(a_s)$.

Third, Fig. 2 shows that $q(a_s; \phi)$ of different directions cross for substrate/lattice mismatch $2\bar{a}_s - a_{\text{eq}} \neq \bar{a}_s + a_{\text{eq}} < 4\%$. For example, while $h001i$ is the softest direction near a_{eq} and stays such upon biaxial expansion (Cu, Ni), it is one of the hardest in biaxially compressed metals (Ag, Au, Cu) where $h201i$ is the softest direction. Similarly, $h111i$ is the hardest direction near the equilibrium and for $a_s = a_{\text{eq}}$, but it becomes softer than $h110i$ and $h201i$ in biaxially expanded Cu and Ni. Thus, there is a qualitative breakdown of the harmonic theory for strains of 4%, and presumably quantitative errors for even smaller strains.

We also note similarities in the elastic behavior of these materials. Under expansion, both Cu and Ni exhibit strong softening of $q(a_s; [001])$ and somewhat weaker softening of $q(a_s; [111])$, while $q(a_s; [110])$ becomes the elastically hardest direction. This order is reversed under biaxial compression of Ag, Au and Cu: q 's for $h001i$ and $h111i$ harden, but the $h110i$ and $h201i$ directions soften.

C. Discussion of anomalous softening of $q(a_s; \phi)$ in terms of fcc/bcc energy differences

The anomalous softening of $q(a_s; [001])$ in Ni and Cu for $a_s > a_{\text{eq}}$ reflects a small fcc/bcc energy difference for these materials. This can be seen by considering three energy surfaces that deform fcc into bcc:

(i) $E(\gamma; V)$: The most general surface is the total energy as a function of the tetragonal shear γ and volume

V , shown as contour in Fig. 4(a) for Cu. The tetragonal shear along $h001i$ is defined by:

$$\epsilon_{ij} = \begin{pmatrix} 0 & 0 & 0 \\ 0 & \frac{1}{2} & 0 \\ 0 & 0 & \frac{1}{2} \end{pmatrix} A; \quad (21)$$

where $c = a = \sqrt{2} \cdot \bar{a}$. $E(\gamma; V)$ has (at least) three extremal points, denoted in Fig. 4(a) as solid dots: one corresponding to the fcc state, one to the bcc state and one to the bct state. These states obey the extremal conditions of vanishing derivatives:

$$\frac{\partial}{\partial \gamma} E(\gamma; V) = \frac{\partial}{\partial V} E(\gamma; V) = 0; \quad (22)$$

Figure 4(a) shows that for Cu fcc and bct are locally stable minima with respect to γ and V , while bcc is a saddle point (maximum with respect to γ and minimum with respect to V).^{64;65}

(ii) Bain path $E(\gamma)$: A more specific function $E(\gamma)$ $E(\gamma; V)|_{V=\text{const}}$ is defined by the tetragonal Bain path,⁶³ connecting fcc and bcc structures. The Bain path is obtained by changing the c/a ratio while keeping $V = ca^2$ constant. When $c/a = 1$ the lattice type is bcc and when $c/a = \sqrt{2}$ it is fcc. The energy as a function of γ must have extremal points at both γ values corresponding to the cubic symmetry fcc ($\gamma_{\text{fcc}} = 1$) and bcc ($\gamma_{\text{bcc}} = 2^{-\frac{1}{2}}$) states, as well as at least another bct point γ_{bct} with a zero derivative $E'(\gamma) = 0$.^{66;67} Usually,^{64;66;68;70} for fcc stable elements the bcc lattice is unstable [i.e., $E(\gamma)$

has a local maximum at b_{cc} and the bct state (a local minimum) occurs for $b_{ct} < b_{cc}$.

(iii) Epitaxial Bain path $E_{eq}(a_s)$: This deformation path is obtained by scanning c while a_s is kept fixed, which corresponds to epitaxial growth on a (001) substrate with lattice parameter a_s . c is determined from the total energy minimization at a fixed a_s :

$$\frac{d}{dc} E_{tot}(c; V) = \frac{2}{3} \frac{1}{c} \frac{\partial}{\partial c} + a_s^2 \frac{\partial}{\partial V} E(c; V) = 0: \quad (23)$$

Eq.(23) defines the epitaxial path $V(c)$, shown as a continuous line in Fig. 4(a). Since $c/a_s = \sqrt{2}^{\frac{1}{2}}$ and $V = ca_s^2 = 4$, this path implicitly relates the out-of-plane dimension c to the substrate lattice constant a_s , much like Eq. (16) does in the harmonic case. As noted in Ref. 65, the epitaxial path crosses all extremal points of $E(c; V)$ because Eq. (23) is satisfied where conditions Eq. (22) hold. Therefore, if we parameterize the epitaxial strain energy along this path as a function of a_s , it has a global minimum corresponding to fcc, a locally stable minimum corresponding to bct and a maximum at the bcc state, see Fig. 4(b). We see that as a_s increases from the equilibrium fcc value, Cu sequentially passes through the bcc and bct states where the strain energy $E^{epi}(a_s; [001])$ is equal to the fcc/bcc and fcc/bct structural energy differences. When these energy differences are much smaller than the characteristic values of the bulk deformation energies $E^{bulk}(a_s)$ [see Fig. 4(b)], then $q(a_s; [001])$ is anomalously soft [since $q(a_s; [001]) = E^{bcc-fcc} = E^{bulk}_{fcc}(a_s)$ for $a_s = (2V_{bcc})^{\frac{1}{3}}$].

In summary, the softness of $q(a_s; [001])$ for $a_s > a_{eq}$ is a reflection of the geometric properties of the h001i epitaxial deformation path (connection between cubic symmetry fcc and bcc structures), and a small fcc/bcc energy difference, $E^{fcc=bcc} = E^{bulk}(a_s)$. It is important that the fcc and bcc points correspond to lattices with cubic symmetry, since it ensures that the energy surface has extremal points there. In zincblende GaP and InP,⁷¹ epitaxial h001i path has only one point of cubic symmetry ($c/a = \sqrt{2}$, corresponding to undistorted fcc), and therefore the energy surface $E(c; V)$ is not required to possess additional extremal points. As a consequence, $E^{epi}(a_s; [001])$ is a monotonously increasing function of a_s , and $q(a_s; [001])$ does not soften with increasing a_s .

The described mechanism also accounts for the softening of $q(a_s; [111])$ for $a_s > a_{eq}$ in Cu and Ni under biaxial h111i expansion, since this deformation takes fcc ($c/a = \sqrt{6}$) into bcc ($c/a = \sqrt{4}$), albeit at a much larger strain. However, we have not found any simple structure corresponding to the compressive h201i strain which could explain the softening of $q(a_s < a_{eq}; [201])$ in Ag, Au and Cu. The latter seems to be caused by relatively loose packing of atoms within the (201) planes, imposing small energy penalty on decreasing the interatomic distances. Indeed, the nearest-neighbor distance in (201) plane is a_s , compared to $a_s/\sqrt{2}$ in (111) or (001) planes with high values of $q(a_s; \phi)$ for $a_s < a_{eq}$.

IV. STABILITY OF SUPERLATTICES AND ALLOYS

A. Constituent strain of superlattices

The bulk formation enthalpy of superlattices [Eq. (8)] is expressed as a sum of the interfacial energy $I(n; \phi)$ and constituent strain energy $E_{CS}^{eq}(x; \phi)$. As given by Eq. (6), the latter is a weighted average of the epitaxial strain energies of coherently strained constituents, minimized with respect to the common in-plane lattice vectors a_1 and a_2 . For the high symmetry directions h001i and h111i, these vectors are related by symmetry operations of the superlattice, so that a_1 and a_2 are proportional to the ideal fcc unit vectors a_1^0 and a_2^0 via Eq. (2). Then $E_{CS}^{eq}(x; \phi)$ can be calculated by minimizing the following expression with respect to the superlattice parameter a_{SL} :

$$E_{CS}^{eq}(x; \phi) = \min_{a_{SL}} (1-x) E_A^{epi}(a_{SL}; \phi) + x E_B^{epi}(a_{SL}; \phi): \quad (24)$$

For lower symmetry directions ϕ , the in-plane unit vectors a_1 and a_2 may relax differently, and the angle $\cos \phi = a_1 \cdot a_2 / |a_1| |a_2|$ is also free to vary. For instance, in h110i superlattices, the vectors a_1 and a_2 are not related by symmetry, and therefore may scale differently, i.e., in ideal fcc $|a_1^0| = |a_2^0| = \sqrt{2}$ but in the superlattice generally $|a_1| \neq |a_2| \notin \sqrt{2}$. Equation (24) is much simpler than the general Eq. (6) requiring minimization with respect to three degrees of freedom: lengths $|a_1|$, $|a_2|$ and the angle $\phi = (a_1^d, a_2)$. In the present work we adopt Eq. (24) even for low symmetry directions, using the calculated $E_A^{epi}(a_s; \phi)$ from Sec. IIIB.

E_{CS}^{eq} : Figure 5 shows the equilibrium constituent strain energies $E_{CS}^{eq}(x; \phi)$ for the size-mismatched Cu-Ag, Ni-Au and Cu-Au systems. They are determined from Eq. (24), using only the epitaxial strain energies $E_{A/B}^{epi}$ of the constituents. There are obvious similarities in $E_{CS}^{eq}(x; \phi)$ for the three noble metal systems. h201i superlattices have the lowest constituent strain energy below $x = 0.2$, after that h001i becomes the softest direction. h111i is the hardest direction over a wide composition range, except close to $x = 1$ where h110i is slightly harder.

This behavior can be explained by the properties of the epitaxial softening function $q(a_s; \phi)$, discussed in Sec. IIIB. For example, consider Cu-Au from Fig. 5. Upon biaxial compression of Au (corresponding to $x < 0.5$), $q(a_s; [111])$ increases rapidly (see Fig. 2), increasing the elastic strain energy and making this an elastically hard direction. In contrast, $q(a_s; [201])$ for Au decreases with biaxial compression, and at $x < 0.2$ there is small energetic penalty for deforming Cu and Au to a common in-plane lattice constant. Increase of $q(a_s; [110])$ for Cu

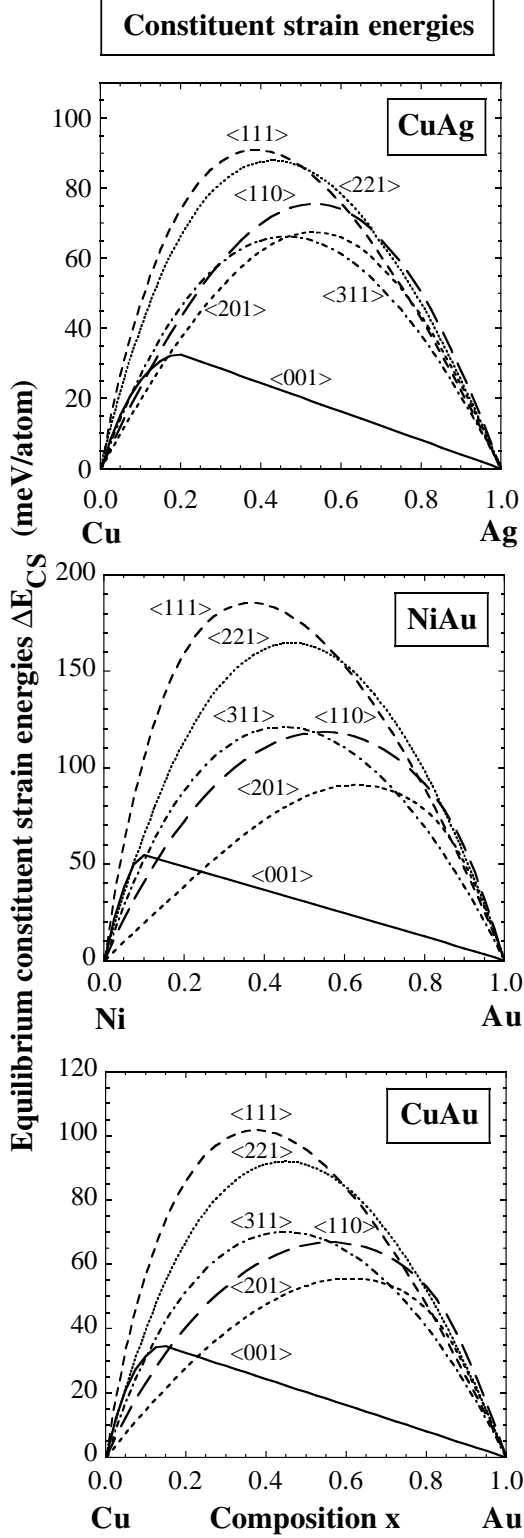


FIG. 5. Equilibrium constituent strain energies for Cu-Au, Ni-Au and Cu-Ag. Ag-Au system is size matched and $E_{CS}^{eq} = 0$.

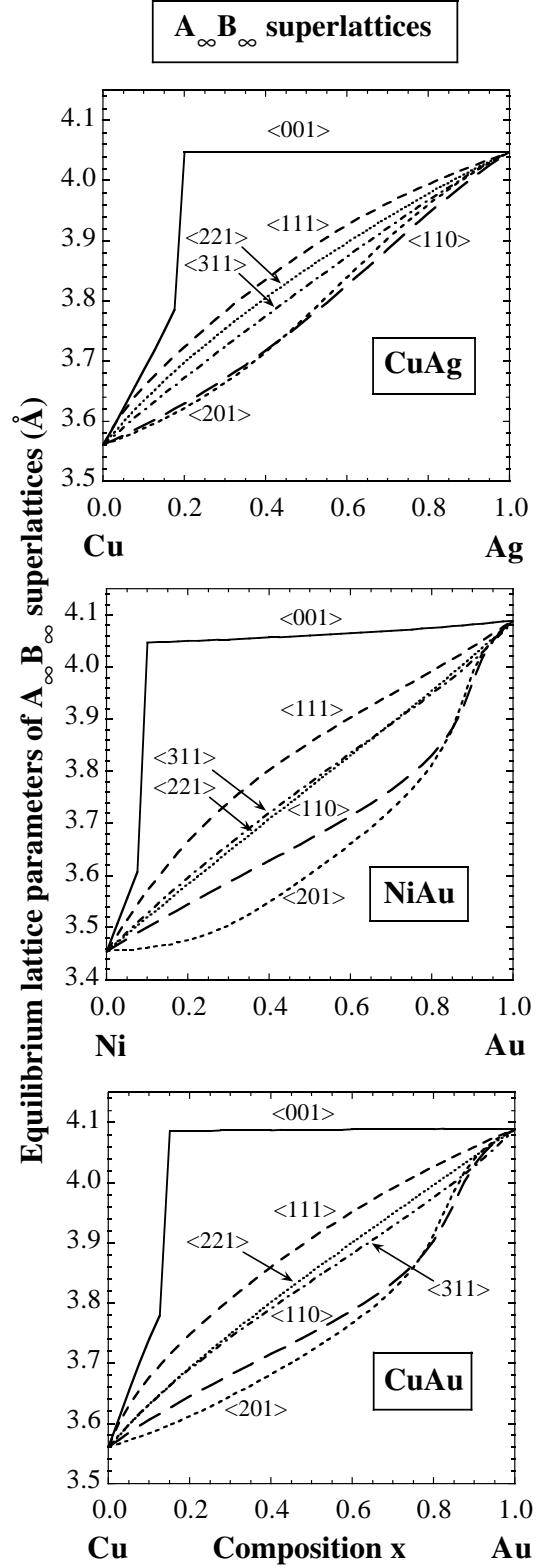


FIG. 6. Equilibrium lattice parameter of infinite Cu-Au, Cu-Ag and Ni-Au superlattices vs composition.

with a_s eventually causes this to be the hardest direction in Au-rich Cu-Au superlattices.

$a_{SL}(x)$: Figure 6 shows the equilibrium in-plane lattice constant $a_{SL}(x; \phi)$ that minimizes the constituent strain. These are also the equilibrium lattice parameters for infinite period superlattices. The lattice parameters $a_{SL}(x; \phi)$ show large deviations from Vegard's law, with the behavior of $a_{SL}(x; [001])$ being particularly anomalous. The very unusual composition dependence of the superlattice parameter for h001i deserves a closer scrutiny: At $x = 0.2$ the superlattice parameter changes discontinuously to the lattice parameter of the larger constituent. The constituent strain energy abruptly changes slope and settles down to a strictly linear composition dependence. Furthermore, $E_{CS}^{eq}(x; [001])$ is very small in comparison with E_{CS}^{eq} for other directions. These anomalies are direct consequences of the soft $q(a_s; [001])$ for biaxially expanded Cu and Ni, which in turn is a consequence of the small fcc/bcc and fcc/bct energy differences for these metals (Sec. IIIB). Indeed, for a sufficiently Au-rich system E_{Cu}^{epi} is smaller than E_{Au}^{epi} favoring a superlattice constant close to the equilibrium lattice parameter of Au. This large lattice parameter happens to fall on the flat region of the strain energy curve around the bcc and bct states of biaxially expanded Cu (see Fig. 4), where a local bct minimum exists in the function on the right-hand side of Eq. (24), shifting downward in energy with increasing x . At some critical value of the composition, the minimum around a_{Au} becomes deeper than the minimum close to a_{Cu} , which causes a discontinuous jump in a_{SL} . Loosely speaking, Cu deforms all the way into the bct structure and Au does not deform at all. That also explains the linear decrease of $E_{CS}(x; [001])$ after the discontinuity, since $E_{Au}^{epi} = 0$ and $E_{Cu}^{epi} = \text{const}$ in Eq. (24).

In conclusion, we summarize the prerequisites for low elastic strain energy of infinite superlattices:

(i) One of the components should exhibit a particularly soft elastic direction under biaxial strain, e.g., h001i in Cu upon epitaxial expansion and h201i in Au upon biaxial compression.

(ii) The lattice mismatch between the constituents should be large enough to explore the regions of anomalous softness.

We stress that the unusual behavior shown in Figs. 6 and 5 (crossing of different directions, discontinuities, different skewnesses of $E_{CS}^{eq}(x; \phi)$ curves) are caused by the anharmonic $q(a_s; \phi)$, and cannot be obtained within the harmonic theory with lattice parameter independent $q_{ham}(\phi)$.⁵⁶

B. Describing chemical interactions via the mixed-space cluster expansion

The energy of a bulk alloy $H_{mix}^{bulk}(x)$ of Eq. (5), and of an epitaxial alloy $H_{mix}^{epi}(x)$ of Eq. (11) cannot be computed directly from LDA since configurationally random structures are involved. The approximate approach is either large supercells or a first-principles mixed-space cluster expansion.^{56;57} In the latter approach, a spin variable S_i is assigned to each lattice site R_i which takes a value ± 1 if the site is occupied by an atom of type A, or ∓ 1 if the site is occupied by an atom of type B. The formation enthalpy of an arbitrary structure is expressed in the following form:

$$H_{CE}(\{S_i\}) = \sum_k J_{pair}(k) \mathcal{S}(k; \{S_i\})^2 + \sum_f D_f J_f \bar{\mathcal{S}}_f(\{S_i\}) + E_{CS}(\{S_i\}); \quad (25)$$

where $J(k)$ is the Fourier transform of real-space pair interactions and $\mathcal{S}(k; \{S_i\})$ is the structure factor,

$$J_{pair}(k) = \sum_j J_{pair}(R_i - R_j) e^{ikR_j}; \quad (26)$$

$$\mathcal{S}(k; \{S_i\}) = \sum_j S_j e^{ikR_j}; \quad (27)$$

The second sum in Eq. (25) runs over symmetry inequivalent clusters constituted by three or more lattice sites. D_f is the number of equivalent clusters per lattice site, and $\bar{\mathcal{S}}_f(\{S_i\})$ are structure-dependent geometrical coefficients (simple lattice averages of the cluster spin products). The last term in Eq. (25) is the constituent strain energy $E_{CS}(\{S_i\})$ of the structure. It is designed to reproduce the elastic strain energy of coherent long-period superlattices⁵⁶ which are calculated directly from the LDA (see Sec. IV A):

$$E_{CS}(\{S_i\}) = \sum_k J_{CS}(x; \mathbf{k}) \mathcal{S}(k; \{S_i\})^2; \quad (28)$$

$$J_{CS}(x; \mathbf{k}) = \frac{E_{CS}^{eq}(x; \mathbf{k})}{4x(1-x)}; \quad (29)$$

The equilibrium constituent strain energies $E_{CS}^{eq}(x; \mathbf{k})$ have been deduced from the directly calculated $E^{epi}(a_{SL}; \phi)$ minimizing Eq. (24) with respect to the common in-plane lattice constant a_{SL} . They are fitted by series of Kubic harmonics with composition dependent coefficients $c_l(x)$:

$$E_{CS}(x; \phi) = \sum_{l=0}^{l_{max}} c_l(x) K_l(\phi); \quad (30)$$

which are used to evaluate $E_{CS}(x; \phi)$ for any direction ϕ . Structure factors $\mathcal{S}(k; \{S_i\})$ in the long-period superlattice limit are nonzero only for $k \neq 0$, where $J_{CS}(x; \mathbf{k})$

is a nonanalytic function of k , reflecting the directional dependence of the constituent strain energy.

The effective cluster interactions J_f and $J_{\text{pair}}(k)$ are determined by fitting Eq. (25) to a large number (30 to 40) fully relaxed first-principles LDA formation enthalpies of simple ordered structures. Most of these ordered structures are short-period superlattices along $h001i$, $h111i$, $h110i$, $h201i$ and $h113i$.⁶⁰ The calculations of $T = 0$ total energies employ the full-potential linearized augmented plane wave method⁶² (FLAPW) and local density approximation (LDA) for the electronic exchange and correlation. The total energy is minimized with respect to all structural degrees of freedom, i.e. both the atomic positions and cell-external coordinates are fully relaxed. Complete discussion of the LDA calculations and cluster expansions for Ag-Au, Cu-Ag, Cu-Au and Ni-Au can be found in Ref. 60.

C. Stability of finite period metal superlattices

Having obtained all ingredients of $H_{\text{CE}}(\phi)$ [Eq. (25)] from LDA calculations on small unit cell structures, we can use this equation to predict the energy of any configuration, in particular superlattices. Figure 7 shows the bulk formation energies of $(A)_n(B)_n$ superlattices for the studied noble metal systems. The interfacial energies $I(n; \phi)$, extracted from $H_{\text{SL}}(n; \phi)$ according to Eq. (8), are shown in Fig. 8. Several interesting observations can be made from these figures:

(i) $I(n; \phi)$ are approximately constant after $n > 5$.

(ii) For ordering systems (Cu-Au and Ag-Au), the interfacial energies are negative (see Fig. 8). Negative interfacial energies are the cause for the upward slope of $H_{\text{SL}}(n; \phi)$ curves in Fig. 7. This indicates a chemical preference for having unlike atoms at the interface and a tendency to form ordered structures at $T = 0$. For instance, $L1_0$, the observed ground state of CuAu, is a monolayer (Cu)/(Au) superlattice along $h001i$. The order of $H_{\text{SL}}(n; \phi)$ is lowest $h001i$ and highest $h111i$ for Cu-Au, and lowest $h110i$ and highest $h111i$ for Ag-Au superlattices.

(iii) For the phase separating Cu-Ag, all interfacial energies are positive. $H_{\text{SL}}(n; \phi)$ decreases with n for all directions and reflect the tendency to coherent phase separation over ordered superlattice formation. Interfaces between Cu and Ag are energetically very costly. The order of $H_{\text{SL}}(n; \phi)$ is again lowest $h001i$ and highest $h111i$.

(iv) Ni-Au has the most interesting behavior of $H_{\text{SL}}(n; \phi)$ and $I(n; \phi)$. It exhibits phase-separating type $H_{\text{SL}}(n; [001])$ (decreasing with n), ordering type $H_{\text{SL}}(n; [110])$ (increasing with n), and a nearly constant $H_{\text{SL}}(n; [111])$. Does this mean that interfaces in some directions are energetically favorable, while in other directions they are energetically costly? The answer is: No. In Ni-Au, just like in Cu-Ag, all isolated

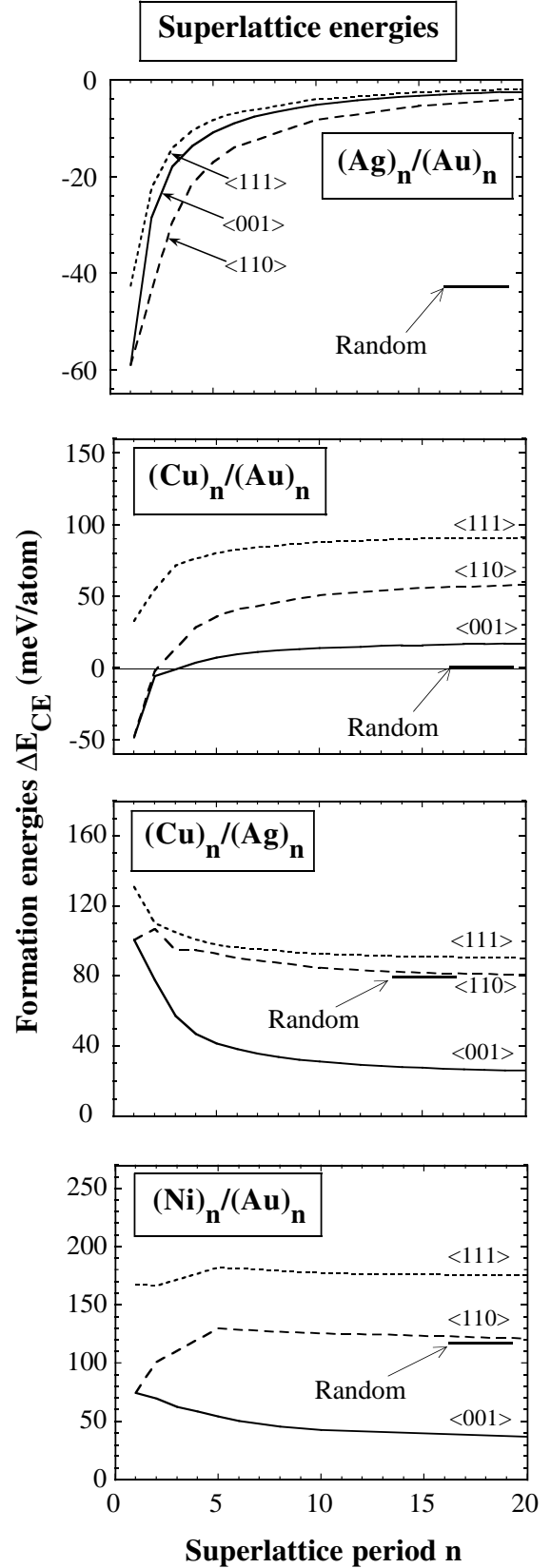


FIG. 7. Superlattice energies for Cu-Au, Cu-Ag, Ni-Au and Ag-Au.

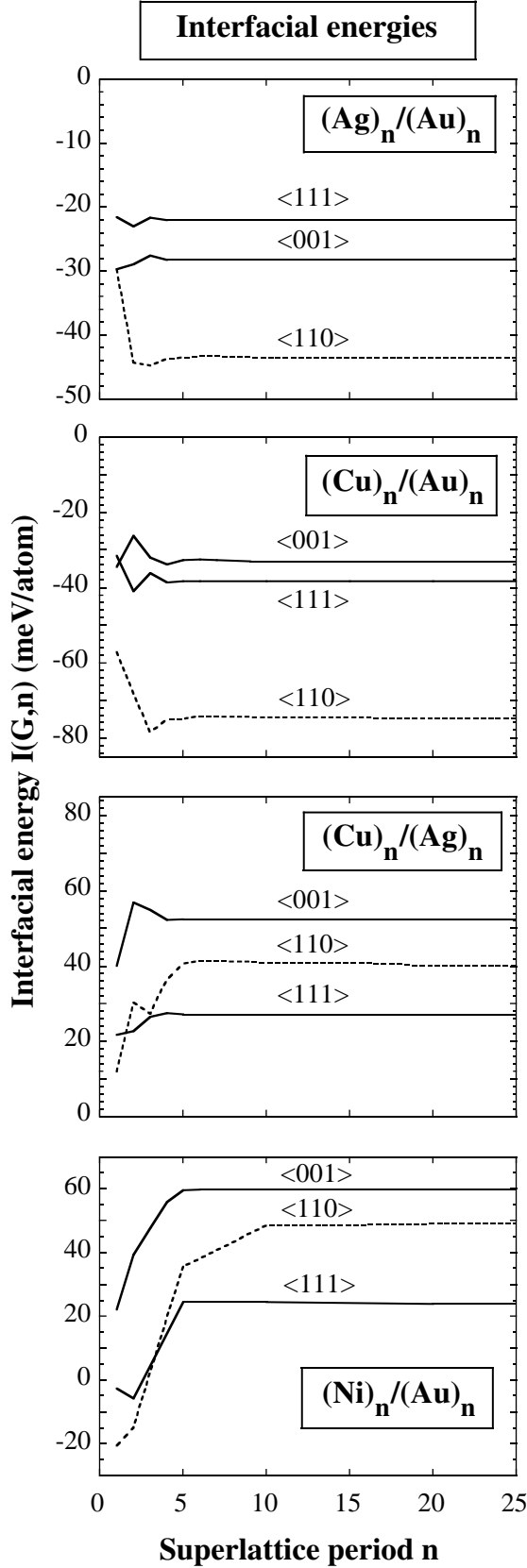


FIG. 8. Interfacial energies of Cu-Au, Cu-Ag, Ni-Au and Ag-Au.

interfaces have positive formation energies. However, the interaction between the interfaces along $h110i$ is strongly attractive in Ni-Au, and leads to a net chemical energy gain for some short-period superlattices. Indeed, Fig. 8 shows that all interfacial energies of Ni-Au are positive in the limit $n \rightarrow 1$ (when there is no interaction between the interfaces), but decrease for short periods and are negative for $h110i$ $n = 3$ superlattices. As we show in Ref. 61 the competition between the constituent strain energy, interfacial energy $I(n \rightarrow 1; \phi)$ and ordering-type interaction between the interfaces leads to unusual short-range order in Ni-Au solid solutions.

(v) It is interesting that in the phase separating Ni-Au and Cu-Ag the lowest interfacial energy $I(n \rightarrow 1; \phi)$ occurs for the close-packed $f111g$ interfaces, and the highest for $f001g$ interfaces. This situation is completely different in the ordering systems Cu-Au and Ag-Au, which have $f110g$ as the lowest and either $f111g$ or $f001g$ as the highest $I(n \rightarrow 1; \phi)$.

(vi) Figure 7 shows the energies of the random alloys at the equiatomic composition. We see that in Cu-Au and Ag-Au all long-period superlattices are unstable with respect to the formation of a random alloy. In Ni-Au the random alloy is less favorable than coherent phase separation in the $h001i$ direction, but slightly more favorable than in $h110i$ coherent superlattices along $h110i$ and $h111i$. However, short-period $h110i$ superlattices are lower in energy than the random alloy. All $h111i$ superlattices of Ni-Au have higher formation enthalpies than the random alloy. In Cu-Ag only the long-period $h001i$ superlattices have lower bulk formation enthalpies than the random alloy. The epitaxial growth of Cu-Ag and Ni-Au alloys is discussed more thoroughly in Sec. IV E.

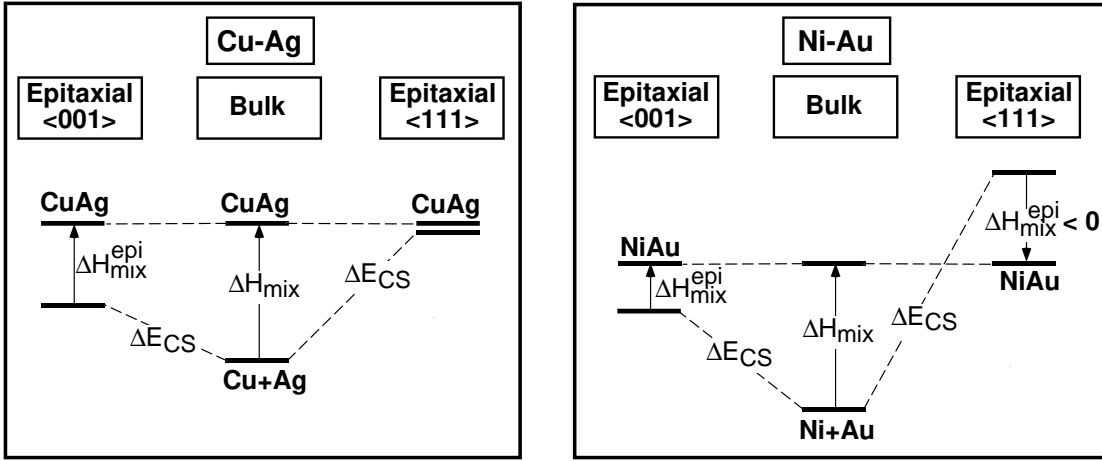
(vii) In size-mismatched systems (Cu-Ag, Cu-Au, and Ni-Au) $H_{SL}(n; \phi)$ exhibit the same order as the constituent strain $E_{CS}^{eq}(x; \phi)$, i.e., $H_{SL}(n; [001])$ is lowest and $H_{SL}(n; [111])$ is highest. It suggests that low constituent strain stabilizes even short-period superlattices.

D. Comparison of the trends in stability of metal and semiconductor superlattices

Growth of semiconductor superlattices is a more mature area than growth of metal superlattices, and much more data are available at present. Thus, it is of interest our results in Figs. 7 and 8 for metals with analogous results for semiconductors.^{72;73}

Lattice-mismatched semiconductors generally have $H_{mix}^{bulk}(x) = 0$ and $H_{SL}^{bulk} = 0$. Thus, they resemble Ni-Au and Cu-Ag rather than the compound-forming system Cu-Au. LDA calculations reveal that $H_{SL}^{bulk}(n; \phi)$ for $G = h111i$ and $G = h001i$ look exactly like in Cu-Ag or Ni-Au: the energy decreases as the period n increases, and the interfacial energies are mostly positive. However, in the $h110i$ and $h201i$ directions, the interfacial energies are negative, and $H_{SL}^{bulk}(n; \phi)$

Calculated Bulk and Epitaxial Energetics in Cu-Ag and Ni-Au



CuAg on (111): Stable, but not at zero temperature

NiAu on (111): Stable!

FIG. 9. Mixing enthalpies H_{mix} (in meV/atom) for bulk and epitaxial equiatomic Cu-Ag and Ni-Au alloys. All epitaxial calculations assume that the substrate is lattice matched to the random alloy. E_{CS} is the sum of epitaxial strain energies of pure elements [see Eq. (11)].

increases with n , like in Ni-Au and Cu-Au. Hence, semiconductor superlattices behave generically as Ni-Au superlattices. However, short-period h201i semiconductor superlattices (e.g., the chalcopyrite structure, corresponding to $n = 2$) have a lower energy than the random alloy, while in Ni-Au it is the h001i short-period superlattices that have lower energies than the random alloy. Hence, while the Ni-Au random alloy can lower its energy by developing h001i ordering, semiconductor random alloys can lower their energy by developing h201i ordering. Both in Ni-Au and semiconductor alloys, the ultimate ground state is incoherent phase separation.

E. Epitaxial growth and surface intermixing

Recent experimental studies^{31,36} have grown epitaxial films of noble metal alloys which are immiscible in the bulk form. For instance, Stevens and Hwang³⁶ have grown Cu-Ag alloys on a Ru(0001) substrate, demonstrating that Cu and Ag are miscible at $T = 823$ K, despite the fact that in bulk, Cu and Ag are strongly immiscible at this temperature and composition. It has also been observed that Au deposited on Ni(110) surface replaces it in the first surface layer forming a surface Ni-Au alloy,³¹ although Au is completely insoluble in bulk Ni. In what follows we show that the stabilization of epitaxial solid solutions from bulk-immiscible con-

stituents can be explained by the additional destabilization of the constituents due to the epitaxial constraint. Indeed, Eq. (11) shows that the epitaxial mixing enthalpy H_{mix}^{epi} may be considerably lower than the bulk mixing enthalpy H_{mix}^{bulk} if the sum of the constituent strain energies on the right hand side is large.

Figure 9 shows the results for the epitaxial stabilization of equiatomic Ni-Au and Cu-Ag alloys, assuming that the substrate is lattice matched to the disordered alloy.

(i) Disordered CuAg and NiAu alloys have large positive bulk mixing enthalpies H_{mix}^{bulk} , in agreement with the observed bulk immiscibility.

(ii) Epitaxy destabilizes the constituents, and hence stabilizes the epitaxial alloy in all cases. This effect is much larger for the elastically hard direction h111i than for the soft h001i direction.

(iii) The epitaxial mixing enthalpy H_{mix}^{epi} for h111i becomes negative in Ni-Au, showing that the solid solution is energetically favored over the epitaxially phase separated state. In CuAg, H_{mix}^{epi} is still positive and these alloys are unstable under epitaxial conditions at $T = 0$ K.

(iv) Epitaxial conditions lead to a significantly enhanced miscibility since $H_{mix}^{epi} < H_{mix}^{bulk}$. A simple mean-field estimate of the miscibility gap temperature for CuAg grown on a nearly lattice-matched Ru(0001) substrate [equivalent to a fcc(111) substrate] gives $T_{MG} = 2 H_{mix}^{epi} = 150$ K. Thus, for (111)-epitaxy at the temperature (823 K) of Steven's and Hwang's experiment,

our calculations predict complete solubility of Cu-Ag, as observed.

(v) The epitaxial stabilization is strongly dependent on the substrate orientation. A bigger effect can be observed for elastically hard directions, e.g., h111i and h110i for noble metal alloys.

V. SUMMARY

We have investigated the effects of anharmonic strain on the stability of epitaxial films, superlattices and epitaxially grown disordered alloys. We find that anharmonic epitaxial strain produces certain qualitative and quantitative features absent in the harmonic theory. In particular,

(i) Epitaxial softening functions $q(a_s; \phi)$ are strongly dependent on the substrate lattice constant a_s , while they are constants in the harmonic theory. For instance, as a consequence of the small fcc/bcc and fcc/bct energy difference, biaxially expanded Cu and Ni show drastic softening of $q(a_s; [001])$. Furthermore, biaxially compressed Cu, Ag, and Au have low values of $q(a_s; \phi)$ along directions h201i and h110i with relatively loose packing of atoms in the epitaxial planes.

(ii) The dependence of $q(a_s; \phi)$ on the direction ϕ can differ from harmonic predictions. For instance, h110i is the hardest direction in biaxially expanded Cu and Ni, and h201i is the softest in biaxially compressed Cu, Ag and Au. The harmonic formula always predicts either h111i as the hardest and h001i as the softest direction, or vice versa.

(iii) The strain energy of infinite coherent superlattices exhibits marked anomalies associated with the anharmonic behavior of constituent $q(a_s; \phi)$. The size-mismatched systems Cu-Ag, Cu-Au and Ni-Au exhibit very low constituent strain for Ag- and Au-rich h001i superlattices, since h001i is the easy direction for biaxial expansion of Cu and Ni. Similarly, h201i superlattices with small Ag or Au content have low coherency strain energies because this is the easy deformation direction for biaxially compressed Ag and Au. The in-plane lattice parameter a_{SL} of long-period h001i superlattices suffers a discontinuous jump around $x \approx 0.2$, and other directions show considerable deviations from linear behaviour.

(iv) These elastic anomalies are less pronounced in short-period superlattices, although they contribute to the structural stability of h001i superlattices. Short-period bulk superlattices are stable in Ag-Au and Cu-Au due to negative interfacial energies. Ag-Au and Ni-Au have positive interfacial energies, leading to superlattice formation being energetically unfavorable with respect to phase separation. The interaction energy between interfaces in Ni-Au is so strong that short-period ($n/2$) superlattices along h110i are more stable than the long-period superlattices with fewer interfaces.

(v) Epitaxially grown disordered alloys can be stabilized even if the system phase separates in bulk form. This effect is caused by additional destabilization of the phase separated state due to the epitaxial constraint on the constituents, requiring them to be coherent with the substrate. The stabilization is more pronounced for elastically hard directions with high values of $q(a_s; \phi)$, e.g. h111i. For instance, we find that even though Ni-Au and Cu-Ag phase separate in the bulk ($H_{mix}^{bulk}(x) > 0$), equiatomic Ni_{0.5}Au_{0.5} alloys are miscible when grown on a lattice-matched (111) substrate, while Cu_{0.5}Ag_{0.5} on a (111) substrate is immiscible at $T = 0$ K but miscible at $T > 150$ K. Neither Ni_{0.5}Au_{0.5} nor Cu_{0.5}Ag_{0.5} are miscible when grown on a lattice-matched (001) substrate, corresponding to a low energy penalty on the phase separated constituents.

ACKNOWLEDGMENTS

This work has been supported by the Office of Energy Research, Basic Energy Sciences, Materials Science Division, U.S. Department of Energy, under contract DE-AC36-83CH10093.

- ¹ D. G. O'Neill and J. E. Houston, Phys. Rev. B 42, 2792 (1990).
- ² M. A. Mueller, E. S. Hirschorn, T. Miller, and T.-C. Chiang, Phys. Rev. B 43, 11825 (1991).
- ³ H. Borne, H. Roder, C. Boragno, and K. Kem, Phys. Rev. B 49, 2997 (1994).
- ⁴ C. Gunther, J. Vrijneth, R. Q. Hwang, and R. J. Behm, Phys. Rev. Lett. 74, 754 (1995).
- ⁵ R. Q. Hwang, J. C. Hamilton, J. L. Stevens, and S. M. Foiles, Phys. Rev. Lett. 75, 4242 (1995).
- ⁶ G. O. Potschke and R. J. Behm, Phys. Rev. B 44, 1442 (1991).
- ⁷ G. Vidali and H. Zeng, Appl. Surf. Sci. 92, 11 (1996).
- ⁸ R. Ramirez, A. Rahman, and I. K. Schuller, Phys. Rev. B 30, 6208 (1984).
- ⁹ E. Bauer and J. H. van der Merwe, Phys. Rev. B 33, 3657 (1986).
- ¹⁰ J. H. van der Merwe, CRC Critical Reviews in Solid State and Materials Sciences 17, 187 (1991).
- ¹¹ F. Gautier and D. Stoeber, Surf. Sci. 249, 265 (1991).
- ¹² C. Mottet, G. Treglia, and B. Legrand, Phys. Rev. B 46, 16 018 (1992).
- ¹³ J. C. Hamilton and S. M. Foiles, Phys. Rev. Lett. 75, 882 (1995).
- ¹⁴ Z. W. Lu, B. M. Klein, and A. Zunger, Superlattices and Microstructures 18, 161 (1995).
- ¹⁵ W. P. Lowe, T. W. Barbee, Jr., T. H. Geballe, and D. B. McWhan, Phys. Rev. B 24, 6193 (1981).

- ¹⁶ I. Banerjee, Q. S. Yang, C. M. Falco, and I. K. Schuller, *Phys. Rev. B* 28, 5037 (1983).
- ¹⁷ C. S. L. Chun, G.-G. Zheng, T. L. Vincent, and I. K. Schuller, *Phys. Rev. B* 29, 4915 (1984).
- ¹⁸ A. Zunger, in *Handbook of Crystal Growth*, Vol. 3, edited by D. T. J. Hurle (Elsevier, Amsterdam, 1994), p. 997, and references therein.
- ¹⁹ C. P. Wang, S. C. Wu, F. Jona, and P. M. Marcus, *Phys. Rev. B* 49, 17 385 (1994).
- ²⁰ A. A. Saleh, V. Shutthanandan, and R. J. Smith, *Phys. Rev. B* 49, 4908 (1994).
- ²¹ S. K. Kim, F. Jona, and P. M. Marcus, *J. Phys. Condens. Matter* 8, 25 (1996).
- ²² H. Womester, E. Huger, and E. Bauer, *Phys. Rev. Lett.* 77, 1540 (1996).
- ²³ E. G. McRae and R. A. M. Alic, *Surf. Sci.* 177, 53 (1986).
- ²⁴ Y. Liu and P. W. ynblatt, *Surf. Sci. Lett.* 241, L21 (1991).
- ²⁵ C. T. Chan, K. P. Bohnen, and K. M. Ho, *Phys. Rev. Lett.* 69, 1672 (1992).
- ²⁶ S. Rousset, S. Chiang, D. E. Fowler, and D. D. Chambliss, *Phys. Rev. Lett.* 69, 3200 (1992).
- ²⁷ D. D. Chambliss and S. Chiang, *Surf. Sci. Lett.* 264, L187 (1992).
- ²⁸ D. D. Chambliss, R. J. Wilson, and S. Chiang, *J. Vac. Sci. Technol. A* 10, 1992 (1993).
- ²⁹ H. Roder, R. Schuster, H. B. nune, and K. Kem, *Phys. Rev. Lett.* 71, 2086 (1993).
- ³⁰ Y. R. Tzeng, H. T. Wu, K. D. Shiang, and T. T. T song, *Phys. Rev. B* 48, 5549 (1993).
- ³¹ L. Pleth Nielsen, F. Besenbacher, I. Stensgaard, E. L. gsgaard, C. Engdahl, P. Stoltze, K. W. Jacobsen, and J. K. N. rskov, *Phys. Rev. Lett.* 71, 754 (1993).
- ³² L. Pleth Nielsen, I. Stensgaard, E. E. L. gsgaard, and F. Besenbacher, *Surf. Sci.* 307-309, 544 (1994).
- ³³ D. O. Boerma, G. Dorenbos, G. H. W. heatley, and T. M. Buck, *Surf. Sci.* 307-309, 674 (1994).
- ³⁴ E. I. Altman and R. J. Colton, *Surf. Sci. Lett.* 304, L400 (1994).
- ³⁵ C. Nagl, M. P. inzolits, M. Schmid, and P. Varga, *Phys. Rev. B* 52, 16 796 (1995).
- ³⁶ J. L. Stevens and R. Q. Hwang, *Phys. Rev. Lett.* 74, 2078 (1995).
- ³⁷ A. K. Schmid, J. C. Hamilton, N. C. Bartelt, and R. Q. Hwang, *Phys. Rev. Lett.* 77, 2977 (1996).
- ³⁸ D. L. Adams, *Appl. Phys.* 62, 123 (1996).
- ³⁹ W. C. Johnson and C. S. Chiang, *J. Appl. Phys.* 64, 1155 (1988).
- ⁴⁰ G. Bozzolo, R. Ibanez-Meier, and J. Ferrante, *Phys. Rev. B* 51, 7207 (1995).
- ⁴¹ J. Terso, *Phys. Rev. Lett.* 74, 434 (1995).
- ⁴² A. Christensen, A. V. Ruban, P. Stoltze, K. W. Jacobsen, H. L. Skriver, and J. K. N. rskov, *Phys. Rev. B* 56, 5822 (1997).
- ⁴³ J. Homstra and W. J. Bartels, *J. Crystal Growth* 44, 513 (1978).
- ⁴⁴ K. Yang, T. A. nan, and L. J. Schowalter, *Appl. Phys. Lett.* 65, 2789 (1994).
- ⁴⁵ P. M. Marcus and F. Jona, *Phys. Rev. B* 51, 5263 (1995).
- ⁴⁶ D. J. Bottomley and P. Fons, *J. of Crystal Growth* 160, 406 (1996).
- ⁴⁷ J. W. Cahn, *Acta Met.* 9, 795 (1961); *ibid.* 10, 179 (1962).
- ⁴⁸ F. C. Larche and J. W. Cahn, *Acta Met.* 33, 331 (1985); *J. Appl. Phys.* 62, 1232 (1987), and references therein.
- ⁴⁹ B. de Cromoux, *J. Phys. Colloq.* 43, C5-19 (1982).
- ⁵⁰ C. P. Flynn, *Phys. Rev. Lett.* 57, 599 (1986).
- ⁵¹ J. B. Stringfellow, *J. Appl. Phys.* 43, 3455 (1972); *J. Electronic Mater.* 11, 903 (1982); *J. Cryst. Growth* 65, 454 (1983).
- ⁵² C. S. Chiang and W. C. Johnson, *J. Mater. Res.* 4, 678 (1989).
- ⁵³ D. M. Wood and A. Zunger, *Phys. Rev. Lett.* 61, 1501 (1988); *Phys. Rev. B* 38, 12 756 (1988); *ibid.* 40, 4062 (1989).
- ⁵⁴ D. M. Wood, *J. Vac. Sci. Technol. B* 10, 1675 (1992), and references therein.
- ⁵⁵ I. P. Ipatova, V. A. Shchukin, V. G. Malyshkin, A. Yu. Maslov, and E. Anastassakis, *Solid State Commun.* 78, 19 (1991); V. G. Malyshkin and V. A. Shchukin, *Semiconductors* 27, 1062 (1993); I. P. Ipatova, V. G. Malyshkin, and V. A. Shchukin, *J. Appl. Phys.* 74, 7198 (1993).
- ⁵⁶ D. B. Laks, L. G. Ferreira, S. Froyen, and A. Zunger, *Phys. Rev. B* 46, 12 587 (1992).
- ⁵⁷ A. Zunger, in *NATO ASI on Statics and Dynamics of Alloy Phase Transformations*, (Plenum Press, New York, 1994), p. 361.
- ⁵⁸ P. Hohenberg and W. Kohn, *Phys. Rev.* 136, 864 (1964); W. Kohn and L. J. Sham, *Phys. Rev. A* 136, 1133 (1965).
- ⁵⁹ S. H. Wei and H. Krakauer, *Phys. Rev. Lett.* 55, 1200 (1985), and references therein. We used the Wigner exchange-correlation functional [E. Wigner, *Phys. Rev.* 46, 1002 (1934)] and equivalent k point meshes [S. Froyen, *Phys. Rev. B* 39, 3168 (1989)] corresponding to 60 points in the irreducible part of the fcc Brillouin zone. (Tests with a 16 × 16 × 16 special points mesh showed negligible differences in the calculated $q(a_s; \Phi)$.) The μ -n-tin radii were $R_{Au} = 2.4a_0$, $R_{Ag} = R_{Cu} = R_{Ni} = 2.2a_0$, and the basis set was defined by $RK_{max} = 9$. Valence states were calculated semi-relativistically (no spin-orbit) [A. H. MacDonald, W. E. Pickett, and D. D. Koelling, *J. Phys. C* 13, 2675 (1980); W. E. Pickett, A. J. Freeman, and D. D. Koelling, *Phys. Rev. B* 23, 1266 (1981)], neglecting electron spin polarization effects. Further details can be found in Ref. 60.
- ⁶⁰ V. O. zolins, C. Wolverton, and A. Zunger, to appear in *Phys. Rev. B* (1998).
- ⁶¹ C. Wolverton and A. Zunger, *Comp. Mater. Sci.* 8, 107 (1997); C. Wolverton, V. O. zolins, and A. Zunger, to appear in *Phys. Rev. B* (1998).
- ⁶² S. H. Wei and H. Krakauer, *Phys. Rev. Lett.* 55, 1200 (1985), and references therein.
- ⁶³ E. C. Bain, *Trans. Am. Inst. Min. Metall. Eng.* 70, 25 (1924).
- ⁶⁴ T. Kraft, P. M. Marcus, M. Methfessel, and M. Scheer, *Phys. Rev. B* 48, 5886 (1993).
- ⁶⁵ P. A. lipp, P. M. Marcus, and M. Scheer, *Phys. Rev. Lett.* 78, 3892 (1997).
- ⁶⁶ M. Sob, L. G. Wang, and V. Vitek, *Comp. Mater. Sci.* 8, 100 (1997).
- ⁶⁷ Indeed, since $E^0(\gamma) < 0$ for γ_{bcc} and $E^0(\gamma) > 0$ for γ_{fcc} , the derivative $E^0(\gamma)$ must pass through zero an odd number of times, proving that in addition to the

two points of cubic symmetry there must exist a third extremal point corresponding to the bct structure. The implicit assumption that there are no inflection points does not change the essence of the discussion.

⁶⁸ P.J.C raievich, M .W einert, J.M .Sanchez, and R .E.W atson, Phys. Rev. Lett. 72 3076 (1994).

⁶⁹ P.J.C raievich, J.M .Sanchez, R .E.W atson, and M .W einert, Phys. Rev. B 55 787 (1997).

⁷⁰ A .Fernandez Guilleme t, V .O zolins, G .G rin vall, and M .K orling, Phys. Rev. B 51, 10 364 (1995).

⁷¹ S.-H .W ei, private communication. In GaP, $q(a_s; [001])$ increases from 0.364 at $a_s = 5.618 \text{ \AA}$ to 0.383 at $a_s = 5.888 \text{ \AA}$, and $q(a_s; [111])$ increases from 0.534 at $a_s = 5.618 \text{ \AA}$ to 0.559 at $a_s = 5.888 \text{ \AA}$.

⁷² R .G .D andrea, J .E .Bernard, S.-H .W ei, and A .Zunger, Phys. Rev. Lett. 64, 36 (1990).

⁷³ S.-H .W ei and A .Zunger, Phys. Rev. Lett. 61, 1505 (1988).